Turbulence Phenomena in a Multiple Normal Shock Wave/ Turbulent Boundary-Layer Interaction

B. F. Carroll*
University of Florida, Gainesville, Florida 32611
and
J. C. Dutton†
University of Illinois at Urbana-Champaign, Urbana, Illinois 61801

An experimental investigation of a Mach 1.61 multiple normal shock wave/turbulent boundary-layer interaction in a rectangular, nearly constant area duct is discussed with an emphasis on the turbulence phenomena. The two-component laser Doppler velocimeter measurements reveal a large amplification of the turbulence kinetic energy and Reynolds stress through the interaction. The leading shock in the multiple shock pattern causes a significant distortion of the turbulent stress tensor. Partial recovery occurs immediately downstream of the first shock. The trailing shocks in the system are much weaker than the first shock and tend to maintain the nonequilibrium turbulence structure, with complete recovery occurring well downstream of the interaction.

Nomenclature

h = duct half height (radius for axisymmetric geometries)
k = turbulence kinetic energy, $(\sigma_u^2 + \sigma_v^2 + \sigma_w^2)/2$
k' = $(u'u' + v'v' + w'w')/2$
M = Mach number
P = pressure
q' = $(u'u' + v'v')$
Re = Reynolds number
T = temperature
U = total velocity
u = streamwise velocity
v = transverse velocity
w = spanwise velocity
x = streamwise direction
y = transverse direction measured perpendicular to wall
z = spanwise direction measured parallel to wall
$\langle\ \rangle$ = ensemble averaged
δ = boundary-layer thickness
σ_u^2 = streamwise normal stress in x direction, $\langle u'u' \rangle$
σ_v^2 = transverse normal stress in y direction, $\langle v'v' \rangle$
σ_w^2 = spanwise normal stress in z direction, $\langle w'w' \rangle$

Subscripts

e = boundary-layer edge
L = local value
u = undisturbed value at station 1
0 = stagnation value

Superscript

$'$ = turbulent fluctuation

Introduction

INTERACTIONS of shock waves with turbulent boundary layers have been studied extensively in the past. Much of the previous work is summarized in the review articles by Adamson and Messiter[1] and by Green.[2] The general interaction may be classified into several broad groups, including oblique shocks in a compression corner, oblique shocks in front of forward facing steps, oblique shocks incident on a flat plate, and normal shocks incident on a flat plate. In an external or unconfined flow, the incident normal shock interaction is characterized by a single normal shock, which is unbifurcated for Mach numbers below about 1.3 and bifurcated for higher Mach numbers. Normal shock/boundary-layer interactions in internal flows are further subjected to the confining effect of the duct walls, as characterized by the ratio of the undistributed boundary-layer thickness to the duct half height (or radius in axisymmetric geometries) δ_u/h. As δ_u/h increases, the character of the interaction changes drastically. With low confinement levels, a single normal shock is formed; for moderate levels of confinement, a multiple or repeated normal shock pattern is obtained; and for high confinement, a repeated oblique shock pattern is found.[3] Increasing Mach number affects the shock structure in a manner similar to increasing confinement.[4] Carroll and Dutton[4] discuss the general characteristics of confined shock wave/turbulent boundary-layer interactions, including Mach number, Reynolds number, and confinement effects. These confined interactions are common in the supersonic, ducted, decelerating flows that occur in several important devices, such as supersonic wind-tunnel diffusers, supersonic gas ejectors, and supersonic and hypersonic inlets.

Several investigations of multiple normal shock wave/turbulent boundary-layer interactions, also called normal shock trains, have been reported. Lustwerk[3] documented the general flowfield characteristics. Ikui et al.[5,6] also discuss general shock train characteristics with an emphasis on the unsteadiness of the interaction. However, these three papers do not present detailed measurements away from the wall. Om and Childs[7] filled this gap by taking detailed pitot-static measurements throughout a Mach 1.49 normal shock train in a circular duct and deducing the mean velocity field from their measurements. Limited mean flow measurements in a moderately confined, planar, Mach 1.6 normal shock interaction have also been obtained by Chriss et al.[8] using a one-component laser Doppler velocimeter (LDV) system. Emphasis was placed on the three-dimensional effects caused by the corners of the duct, and the existence of a multiple shock system was not fully investigated. All of these investigations of normal shock trains have been limited to mean flow data, with the exceptions of Ikui et al.,[6] who presented fluctuating wall static pressure results, and Chriss et al.,[8] who obtained one-component, noncoincident turbulence data.

Received Aug. 20, 1990; revision received Dec. 10, 1990; accepted for publication Jan. 22, 1991.

*Assistant Professor, Department of Aerospace Engineering, Mechanics & Engineering Science. Member AIAA.
†Professor, Department of Mechanical and Industrial Engineering. Associate Fellow AIAA.

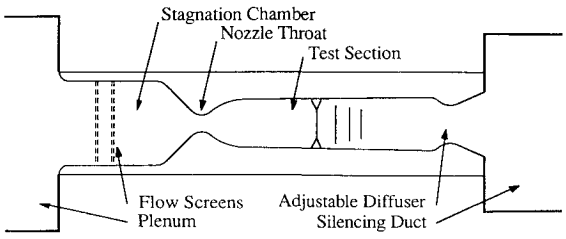

Fig. 1 Schematic of the small-scale supersonic wind tunnel/test section.

Two-component LDV measurements, including turbulence data, for several related single normal shock/boundary-layer interactions have been reported.[9-11] Sajben et al.[9] considered a confined normal shock/boundary-layer interaction in an inlet geometry with a downstream adverse pressure gradient, i.e., with a diverging duct downstream. The level of flow confinement was lower than in the present work. Normal shock/boundary-layer interactions at even lower confinement levels were investigated by Delery[10] and East.[11] Using pitot probes and hot-wire anemometry, Mateer et al.[12] obtained mean and fluctuating velocity data from a moderately confined single normal shock/turbulent boundary-layer interaction. Detailed mean and fluctuating velocity measurements in a highly confined, multiple normal shock/turbulent boundary-layer interaction have not been previously reported and are the subject of the present investigation.[13] In a Mach 1.6 normal shock train in a rectangular cross section, nearly constant area duct was investigated using spark schlieren photography, mean wall pressure measurements, and two-component LDV. The mean flow LDV measurements have been treated in a separate paper.[14] The present paper considers the turbulent flow phenomena in this Mach 1.6 normal shock train.

Experimental Apparatus

All experiments reported here were performed in the Gas Dynamics Laboratory at the University of Illinois at Urbana-Champaign. A complete discussion of this facility is given by Carroll and Dutton.[4,13,14] A schematic of the small-scale, planar two-dimensional supersonic wind tunnel used in this investigation is shown in Fig. 1. Wire mesh screens and honeycomb, installed upstream of the screens but not shown in the schematic, condition the flow before it passes through the symmetric supersonic nozzle. The test section begins at the nozzle exit and extends for 753.8 mm (29.67 in.) downstream. It consists of a rectangular duct with a constant width of 76.2 mm (3.0 in.). The upper and lower test section walls each have a divergence angle of 0.13 deg to allow for boundary-layer growth. The divergence begins at the nozzle exit where the duct height is 32.06 mm (1.262 in.). Optical access to the test section is provided by removable windows in the tunnel side walls. An adjustable converging-diverging diffuser is mounted at the test section exit and is used to impose an elevated downstream pressure level that forces the shock train into the duct. Static pressure taps are located along the centerline of the upper and lower test section walls with a minimum spacing of 12.7 mm (0.5 in.). No provisions were made to measure high-frequency fluctuations in the wall pressure.

The experimental techniques consisted of both qualitative flow visualizations and quantitative pressure and LDV measurements. The main instrumentation was a two-component, dual-beam, coincident, forward scatter, frequency shifted LDV system. A complete description of the LDV system, including operating procedures, counter settings, data reduction, and a thorough discussion of the experimental uncertainty, is given by Carroll and Dutton.[13,14] Because of the complexity of the LDV measurements and data reduction, a simple error band cannot be specified. The combined effects of several mutually interacting error sources must be considered at each point. The LDV measurement volume diameter was 0.08 mm. The seed particles, atomized 50-cp silicone oil, have an average diameter of 0.8 μm and have sufficient frequency response to follow the turbulent fluctuations.[13] A coincidence window of 1–2.5 μs, depending on the local mean velocity, was required for the two-component measurements. The measurements are best described as low burst density, i.e., a low probability of having more than one particle in the measurement volume at a time, and low data density, i.e., the time between successive samples is large compared to the time scale of the turbulent fluctuations. Since the sampling rate was too low to resolve the actual time history of the velocity field, all turbulence information is obtained via ensemble averages of the 4096 instantaneous velocity realizations taken at each measurement point. The ensemble averaged statistical results were corrected for velocity bias using a two-dimensional velocity inverse weighting. Fringe bias effects were found to be negligible.

Results

The experimental results will now be discussed. All LDV measurements reported here were made along the test section midplane in the bottom half of the duct to take advantage of the symmetric nature of the interaction. At the start of the interaction, the centerline was located at $y = 16.875$ mm from the wall. The two-component measurements were made from just above the tunnel centerline down to $y = 1.25$ mm. One-component measurements were then made from $y = 1.25$ to 0.10 mm, which lies within a distance of $y^+ = 100$ from the wall. The one-component measurements only yield information on the streamwise mean velocity u and the streamwise fluctuating velocity u'. The operating conditions were the following: stagnation pressure $P_0 = 206 \pm 0.7$ kPa; stagnation temperature $T_0 = 295 \pm 2$ K; and unit Reynolds number $Re/m = 30 \times 10^6$ m^{-1}. A fixed shock train location in the test section was maintained by adjusting the downstream diffuser. At this shock train location, the undisturbed Mach number just upstream of the interaction was $M_u = 1.61$, the undisturbed boundary-layer thickness was $\delta_u = 5.4$ mm, and the confinement level was $\delta_u/h = 0.32$.

Transverse traverses were made at the 26 streamwise stations listed in Table 1. The first 21 measurement stations are

Table 1 Measurement stations

Station	$(x - x_u)/\delta_u$
1	0.0
2	1.39
3	2.78
First shock	
4	3.70
5	4.17
6	4.63
7	5.09
8	5.56
9	6.02
10	6.48
11	6.94
12	7.41
Second shock	
13	8.33
14	8.80
15	9.26
16	9.72
17	10.2
18	10.6
Third shock	
19	12.0
20	13.9
21	17.6
22	27.8
23	37.0
24	46.3
25	60.2
26	74.1

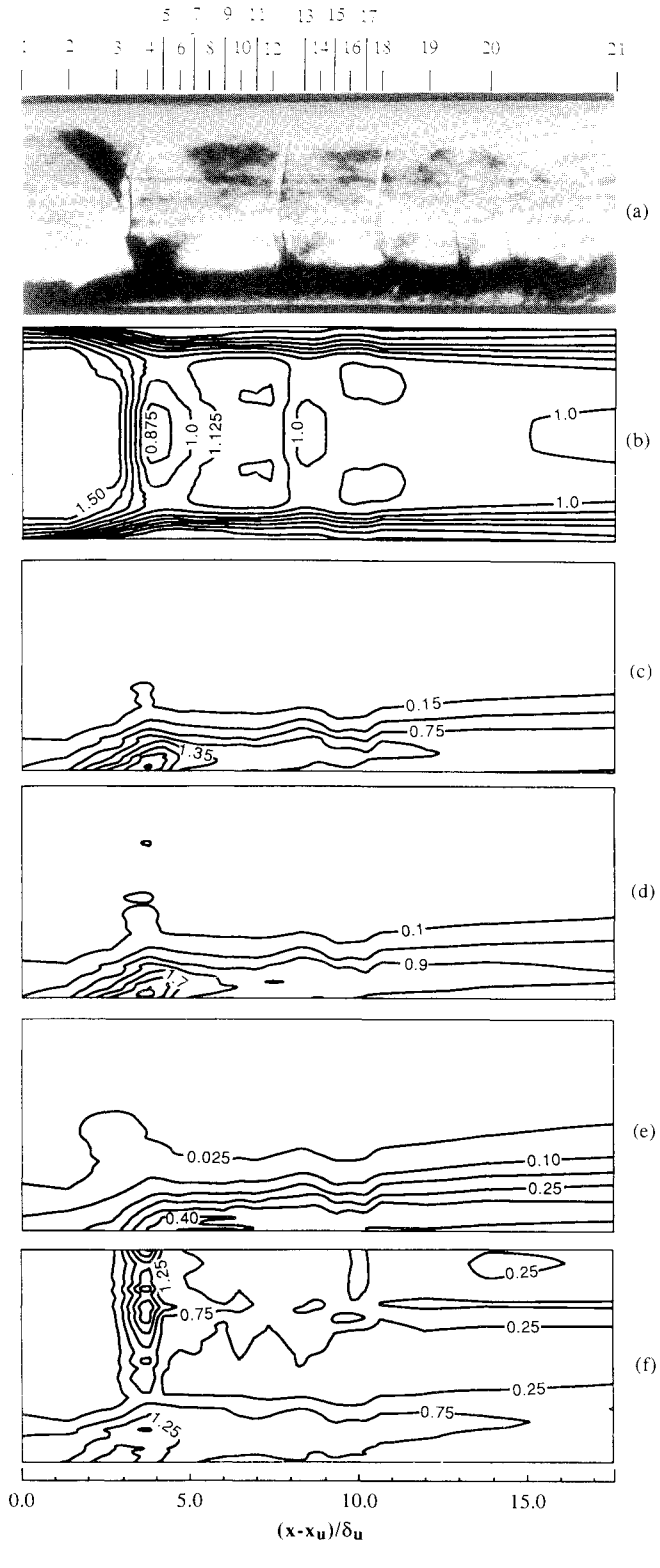

Fig. 2 Schlieren photograph and LDV contour plots, flow from left to right: a) schlieren with horizontal knife edge; b) Mach number; c) turbulence kinetic energy, $k/U_{ue}^2 \times 10^2$; d) streamwise normal stress, $\sigma_u^2/U_{ue}^2 \times 10^2$; e) transverse normal stress, $\sigma_v^2/U_{ue}^2 \times 10^2$; f) anisotropy ratio, $\sigma_u/\sigma_v - 1$.

also shown at the top of Fig. 2a, which is a spark schlieren photograph of the normal shock train with the flow from left to right. Measurements were concentrated in the regions between the first and second shocks and between the second and third shocks. This was done to document the flow following each major type of shock appearing in the normal shock train; the first shock is bifurcated, whereas the weaker trailing secondary shocks were unbifurcated. The spacing between the shocks decreases following each successive shock in the system. A slip line is generated at the bifurcation point of the first shock ($y/\delta_u = 2.3$) and extends downstream though the trailing shocks. Substantial thickening of the boundary layer is observed through the interaction with the quickest growth occurring below the bifurcated first shock. The schlieren results are valuable in gaining a qualitative knowledge of the flow. A more quantitative understanding of the normal shock train will now be developed from the LDV measurements.

The Mach number distribution through the interaction is given in the contour plot of Fig. 2b. The Mach number contour plot differs from the other contour plots of Figs. 2 and 3 in that the data have been reflected about the centerline to give a symmetric plot. In all subsequent contour plots, only the bottom half of the flow is shown. The Mach number ranges from a maximum value of 1.61 in the core flow upstream of the first shock to a minimum of 0.80 along the centerline following the first shock. This Mach number is higher than the value of 0.67 predicted by the standard one-dimensional normal shock relations. There are two probable causes for this. Some particle lag is present at stations 4 and 5 following the normal part of the first shock. Although these effects are small, they do cause the measured particle velocity to be somewhat higher than the actual flow velocity.[14] Additionally, the flow following the outer nearly normal portion of the first shock immediately begins to reaccelerate.[14] The slight curvature of the normal shock causes the mean velocity vector to point toward the centerline forming an aerodynamic nozzle effect. A region of supersonic flow exists near the boundary-layer edge following the bifurcation. In unconfined single normal shock/boundary-layer interactions, this region is normally termed a supersonic tongue. In a confined interaction, the supersonic tongue grows filling the entire core flow before the second shock is reached. The notches seen in the Mach number contour lines, downstream of the bifurcation point, correspond to the slip line seen in the schlieren, Fig. 2a. Just prior to the second shock (station 12), the Mach number is 1.23 inside the slip line and 1.26 outside the slip line. A subsonic region also exists following the second shock with the minimum Mach number being 0.93 at station 13. The flow is totally subsonic after approximately four duct heights downstream of the interaction. Under the first shock, the boundary layer is incipiently separated. The high level of flow confinement tends to delay separation until higher incoming Mach numbers than one would expect in an unconfined interaction.[14,15] The weaker secondary shocks also fail to separate the boundary layer but do delay the full recovery of the turbulence field of the nearly separated boundary layer until downstream of the interaction.

The remainder of this paper will focus on the turbulence properties of the Mach 1.61 shock train. Figure 2c presents the dimensionless turbulence kinetic energy k/U_{ue}^2, where $k = (\sigma_u^2 + \sigma_v^2 + \sigma_w^2)/2$, $\sigma_u^2 = \langle u'u' \rangle$, $\sigma_v^2 = \langle v'v' \rangle$, and $\sigma_w^2 = \langle w'w' \rangle$. In this study, the spanwise normal stress σ_w^2 was estimated as $\sigma_w^2 = (\sigma_u^2 + \sigma_v^2)/2$, making $k = 0.75(\sigma_u^2 + \sigma_v^2)$. The core flow turbulence kinetic energy is below the minimum measurable level. The uncertainty due to the counter clock resolution of ± 1 ns is manifested as an apparent turbulent fluctuation that limits the minimum measurable turbulence kinetic energy. In the core flow ahead of the first shock, the uncertainty in σ_u and σ_v is $<1\%$ of the local u and v velocity components, respectively, and it is $<0.7\%$ downstream of the first shock. A large amplification and local maximum in k is observed under the foot of the bifurcated first shock. The trailing shocks do not appear to increase k. Rather, they tend to maintain the turbulence kinetic energy at elevated levels relative to the incoming boundary layer. The turbulence kinetic energy does not diffuse outside the boundary layer until downstream of the interaction. Diffusion

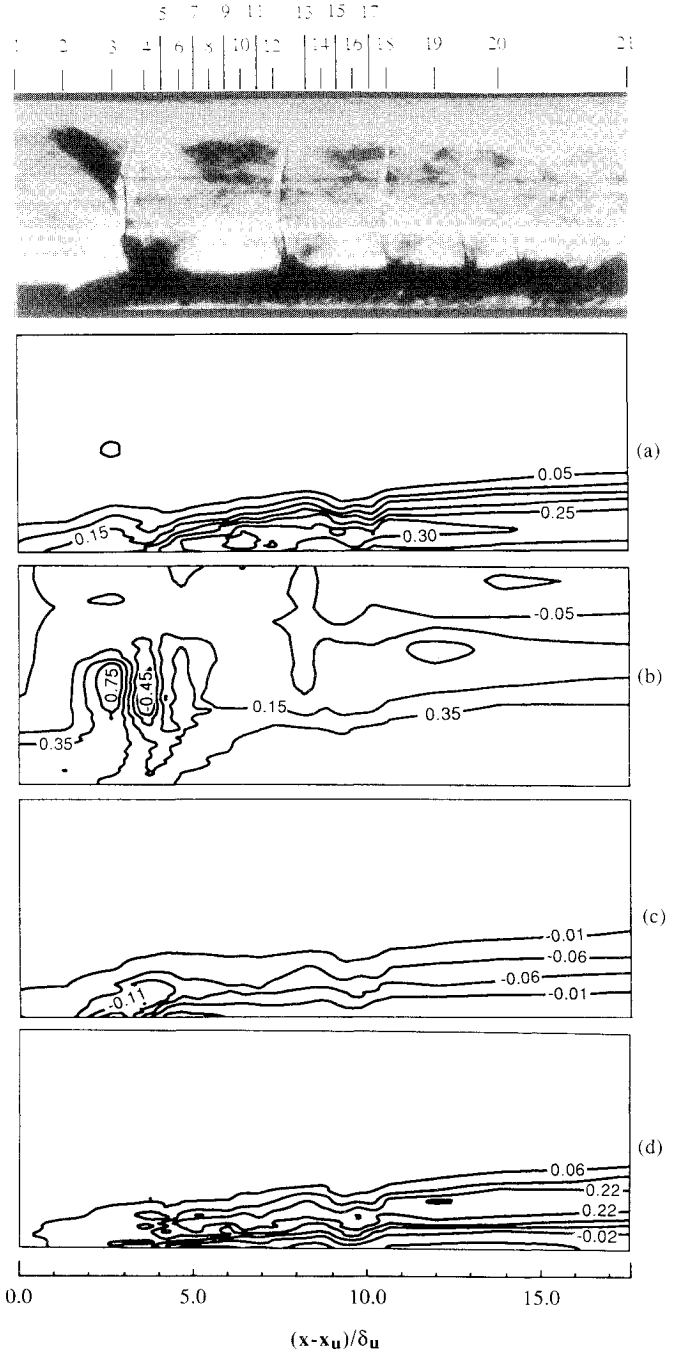

Fig. 3 LDV contour plots, flow from left to right (schlieren photograph at top): a) Reynolds shear stress, $-\langle u'v'\rangle/U_{ue}^2 \times 10^2$; b) shear stress correlation coefficient, $-\langle u'v'\rangle/(\sigma_u\sigma_v)$; c) triple velocity correlation component, $(\langle u'q'\rangle/U_{ue}^3) \times 10^2$; d) triple velocity correlation component, $(\langle v'q'\rangle/U_{ue}^3) \times 10^3$.

of k (from the boundary layer) across the slip line does not occur until station 24. The streamwise distribution of the peak value of the dimensionless turbulence kinetic energy k/U_{ue}^2 is plotted in Fig. 4. A factor of 3.8 increase in this peak value occurs at the first shock. Following the first shock, a nearly constant peak level of 2.5 times the incoming value is maintained until the end of the interaction. In the incoming boundary layer, the peak value of k occurs below the closest two-component measurement location ($y^+ = 727$, $y/\delta_u = 0.23$). The location of the peak then moves progressively farther away from the wall, ranging from $y/\delta_u = 0.35$ to 0.45 through the second shock and increasing to $y/\delta_u = 0.55$ at station 21. The turbulence kinetic energy distribution has begun to resemble equilibrium conditions by station 26 with the maximum value of k being 0.60 times that in the incoming boundary layer. The turbulence kinetic energy normalized by the local velocity squared k/U_L^2 behaves similarly to k/U_{ue}^2 with two major exceptions. First, the magnitude of the amplification through the first shock is much greater, with a factor of 40 increase in the local value. Second, the peak local turbulence intensity occurs much closer to the wall than the peak in k alone since the square of the local velocity decreases at a faster rate than k as the wall is approached.

The streamwise Reynolds normal stress σ_u^2 is the major contribution to the turbulence kinetic energy and, therefore, behaves quite similarly to k. However, σ_u^2 is obtained from both the one- and two-component LDV optical setups, allowing σ_u^2 measurements down to $y = 0.10$ mm ($y/\delta_u = 0.02$). The contour plot for $(\sigma_u/U_{ue})^2$, Fig. 2d, is very similar to that for k/U_{ue}^2, Fig. 2c. A larger region of high values is observed under the bifurcation, and elevated levels of $(\sigma_u/U_{ue})^2$ are present at the slip line (but are not evident in the contour plot). The dimensionless transverse normal stress $(\sigma_v/U_{ue})^2$ is shown in Fig. 2e. The amplification in σ_v^2 begins slightly downstream of the corresponding increase in σ_u^2. A localized maximum in σ_v^2 appears at the bifurcation point, and the high levels of σ_v^2 also tend to persist further downstream in the near wall region. In this near wall region downstream of the bifurcated first shock, the mean flow results show that a transverse mass flux toward the wall occurs as the boundary layer recovers from a nearly separated state. The transverse normal stress is small at the slip line. The distributions of the peak values in $(\sigma_u/U_{ue})^2$ and $(\sigma_v/U_{ue})^2$ given in Fig. 5 emphasize these points. The transverse locations of the peak values of

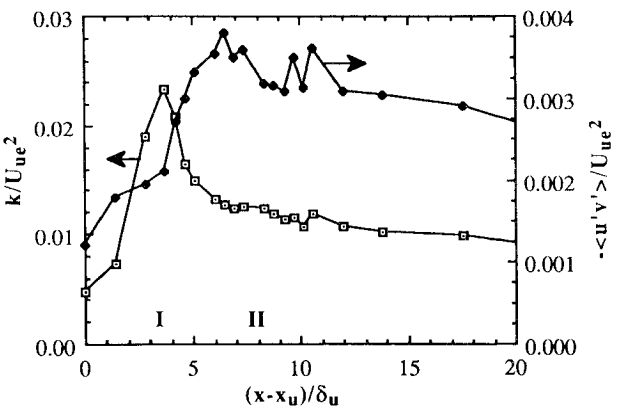

Fig. 4 Distribution of peak values of turbulence kinetic energy, k/U_{ue}^2, and Reynolds shear stress, $-\langle u'v'\rangle/U_{ue}^2$, with location of first and second shocks denoted by I and II, respectively.

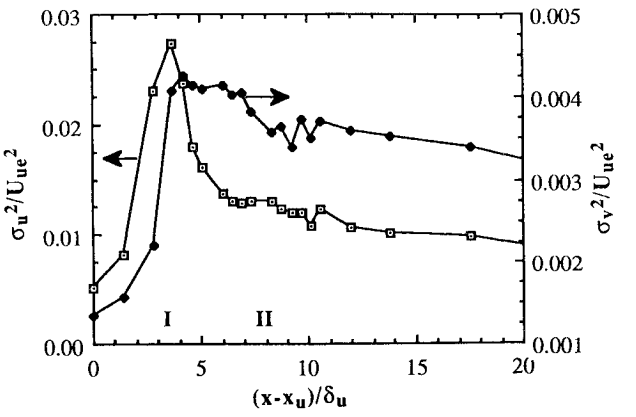

Fig. 5 Distribution of peak values of streamwise and transverse normal stress components, $(\sigma_u/U_{ue})^2$ and $(\sigma_v/U_{ue})^2$, with location of first and second shocks denoted by I and II, respectively.

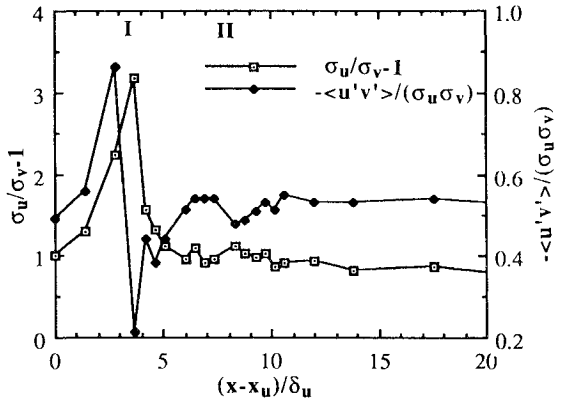

Fig. 6 Distribution of peak values of anisotropy ratio, $\sigma_u/\sigma_v - 1$, and shear stress correlation coefficient, $-\langle u'v'\rangle/(\sigma_u\sigma_v)$, with location of first and second shocks denoted by I and II, respectively.

streamwise and transverse velocity range between $y/\delta_u = 0.35$–0.55. The transverse normal stress rises sharply through the first shock, then stays at high levels seeing only a gradual decrease farther downstream. In contrast, the streamwise normal stress undergoes a local maximum under the first shock, then trails off quickly before undergoing a more gradual decay downstream. Comparing the maximum observed values, the maximum streamwise normal stress $(\sigma_u/U_{ue})^2$ is approximately 6.5 times the transverse value. One might speculate that part of this large localized increase in the streamwise component is actually a false turbulence due to small-scale, high-frequency shock motion similar to that observed by Dolling and Murphy[16] in an oblique shock/boundary-layer interaction at a compression corner. Conclusive evidence regarding this hypothesis was not obtained in the current experiments. High-frequency wall static pressure measurements were not available, and the velocity histograms from the LDV measurements at the foot of the bifurcation do not have bimodal distribution, which indicates that large-scale shock motion was not present, but does not preclude small-scale, high-frequency shock motion. Unequal deceleration of the polydispersed seed particles could also cause a false turbulence. A positive skewness in the core flow data at stations 4–6 is probably due to this effect. However, such a skewness is not seen in the boundary layer, indicating that the nonuniform particle size distribution has only a small influence on the amplification of $(\sigma_u/U_{ue})^2$ seen within the boundary layer.

The relative magnitudes of σ_u and σ_v have implications in turbulence modeling since many models are based on equilibrium distributions of these quantities. The anisotropy ratio, defined by $(\sigma_u/\sigma_v - 1)$, is given in Fig. 2f. A high level of anisotropy is seen to exist near the outer portion of the bifurcated first shock. This is probably due to small-scale shock motion and particle lag effects. Relatively high anisotropy also occurs near the slip line, where u is changing rapidly but v remains constant. The region of true interest is near the wall in the boundary layer. A large increase in anisotropy occurs at the foot of the bifurcated shock. Then, the anisotropy ratio returns to near equilibrium levels for the remainder of the flow. Delery[10] noticed a similar increase in anistropy in an unconfined single normal shock interaction. He attributed this to the relative magnitude of the production terms for σ_u and σ_v. The shock/boundary-layer interaction enhances production of σ_u while decreasing production of σ_v. The streamwise distribution of the peak value of $(\sigma_u/\sigma_v - 1)$ is given in Fig. 6, where a factor of 3 increase is seen to occur under the first shock. The peak levels of anisotropy at each streamwise station are seen to be slightly lower in the later regions of the interaction than in the incoming flow and continue to decrease slowly in the redeveloping flow all the way to station 26.

The dimensionless kinematic turbulent shear stress, or Reynolds shear stress, defined as $-\langle u'v'\rangle/U_{ue}^2$ in a two-dimensional flow, is presented in Fig. 3a. The negative sign is included since u' and v' tend to be negatively correlated in an equilibrium boundary layer. An increase and subsequent decrease in the Reynolds shear stress is seen to occur near the bifurcation point and could be attributed to small-scale shock motion. The leading leg of the bifurcation decreases u but increases v, such that shock motion would lead to a negative correlation between u' and v' and would increase the Reynolds shear stress. Conversely, the trailing leg decreases both u and v, such that small-scale shock motion would decrease the Reynolds shear stress. Amplification of the Reynolds shear stress occurs in the near wall region of the boundary layer, beginning under the bifurcation and continuing downstream of the bifurcated shock. Reference to Fig. 4 shows that the location of maximum Reynolds shear stress within the boundary layer occurs approximately $2.5\delta_u$ downstream of the peak in k. The maximum in $-\langle u'v'\rangle/U_{ue}^2$ is 3.2 times the peak value in the incoming boundary layer. Downstream, the Reynolds shear stress slowly decreases until, at station 26, $-\langle u'v'\rangle/U_{ue}^2$ is only 0.5 times the maximum value at station 1. The high levels of Reynolds shear stress also persist farther downstream than the high levels of turbulence kinetic energy.

As was mentioned earlier, the relative magnitude of the kinematic turbulent normal stresses σ_u^2 and σ_v^2 is an important consideration in turbulence modeling. The relative magnitude of the turbulent shear stress to the turbulent normal stresses is also important. The stress correlation coefficient $-\langle u'v'\rangle/(\sigma_u\sigma_v)$ is a useful parameter to investigate these effects. As shown in Fig. 3b, the stress correlation coefficient remains at levels comparable to those in the incoming boundary layer, except in the region of the first shock. Near the bifurcation point, a large increase and subsequent decrease occur. This may be caused by the previously discussed influence of small-scale shock motion on the Reynolds stress. Near the wall, a decrease in the stress correlation coefficient occurs near the trailing leg of the bifurcation. The values in the core flow may be erroneous due to the near zero levels of the turbulent stresses involved in forming the stress correlation coefficient. Thus, the region of true concern, from the standpoint of turbulence modeling, is near the wall in the vicinity of the trailing leg of the first shock. The peak values of the stress correlation coefficient at each streamwise location are plotted in Fig. 6. After some oscillations in the vicinity of the first shock, nearly constant levels, close to that in the incoming boundary layer, are maintained for the remainder of the interaction and downstream in the recovering boundary layer.

The turbulent diffusive transport terms, which arise in the turbulence kinetic energy equation, include pressure-gradient work, transport by turbulent velocity fluctuations, and transport by viscous stresses. At high Reynolds numbers, the transport by viscous stresses is generally negligible. The pressure work term is often neglected as well, leaving the turbulent velocity fluctuations as the main diffusive mechanism. Their net effect is to redistribute the turbulence kinetic energy both to different physical locations and to different wave numbers. In the transport equation for k, the diffusion of turbulence kinetic energy by streamwise velocity fluctuations is given by $\partial\langle u'k'\rangle/\partial x$, where $k' = (u'u' + v'v' + w'w')/2$, and the diffusion of turbulence kinetic energy by transverse velocity fluctuations is given by $\partial\langle v'k'\rangle/\partial y$. Since the w' fluctuations were not measured in the present study, the behavior of the triple velocity correlations $\langle u'q'\rangle$ and $\langle v'q'\rangle$, with $q' = u'u' + v'v'$, was examined to investigate the relative importance of diffusive transport effects in the flow. A contour plot of $\langle u'q'\rangle/U_{ue}^3$ is given in Fig. 3c. This term has a negative value in the incoming boundary layer and decreases to even lower values under the foot of the first shock. The large amplification in the absolute value begins near the trailing leg and is maintained in a narrow band of the outer portion of the

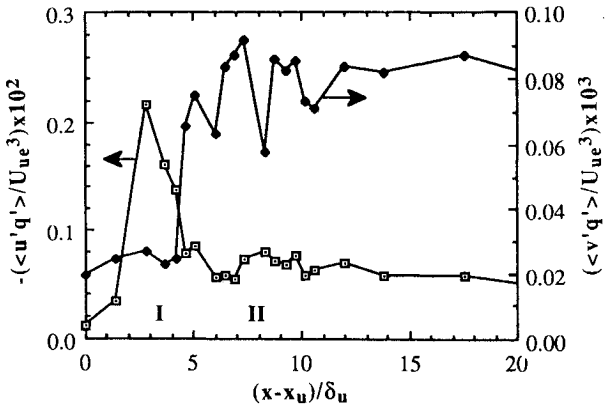

Fig. 7 Distribution of peak values of $\langle u'q'\rangle/U_{ue}^3 \times 10^2$ and $\langle v'q'\rangle/U_{ue}^3 \times 10^3$, with location of first and second shocks denoted by I and II, respectively.

boundary layer for the remainder of the interaction. The $\langle v'q'\rangle/U_{ue}^3$ contour plot is given in Fig. 3d. In contrast to $\langle u'q'\rangle$, $\langle v'q'\rangle$ is positive in the incoming boundary layer. A large amplification of $\langle v'q'\rangle$ begins near the wall slightly downstream of the trailing leg with the high values maintained in a fairly wide band in the outer portion of the boundary layer for the remainder of the interaction. The absolute values of both $\langle v'q'\rangle$ and $\langle u'q'\rangle$ are damped near the wall in the later stages of the interaction with $\langle v'q'\rangle$ actually reaching slightly negative values near the wall. Figure 7 shows the streamwise distributions of the peak values of $-\langle u'q'\rangle/U_{ue}^3$ and $\langle v'q'\rangle/U_{ue}^3$. A large localized increase in $-\langle u'q'\rangle/U_{ue}^3$ occurs under the first shock before returning to nearly constant values in the later stages of the shock train. In contrast, the peak values of $\langle v'q'\rangle/U_{ue}^3$ increase rapidly just downstream of the trialing leg of the bifurcated shock, then remain at nearly constant levels for the remainder of the interaction. The absolute magnitude of the peak values of $\langle u'q'\rangle/U_{ue}^3$ are roughly 3 times greater than that of $\langle v'q'\rangle/U_{ue}^3$. These results imply that diffusive transport of turbulence kinetic energy is an important mechanism both within the interaction and downstream in the redeveloping boundary layer.

Conclusions

The results presented here demonstrate that large deviations from the incoming equilibrium boundary-layer turbulence structure occur through the normal shock train. The largest deviations occur beneath the bifurcated first shock where the turbulence is more elliptic than isotropic in nature. The stress correlation coefficient is also significantly disturbed in this region. Both the level of anisotropy and the stress correlation coefficient return to near equilibrium levels prior to the second shock. A large increase in turbulence kinetic energy occurs at the first shock with the weaker trailing shocks tending to maintain this high level of turbulence. In the recovering boundary layer downstream, a slow diffusion of the turbulence kinetic energy into the core flow occurs. Triple velocity correlations experience elevated levels in the outer part of the boundary layer following the first shock and are damped in the inner parts of the boundary layer. Proper modeling of the turbulence structure in this interaction must take into account the perturbations to the turbulence field discussed earlier. In particular, isotropic turbulence models would be expected to perform poorly at the foot of the first shock but may perform adequately in the later stages of the shock train.

Acknowledgments

This work was supported by the Office of Naval Research Contract N00014-85-K-0665 monitored by Spiro Lekoudis. Additional support was provided by an Office of Naval Research Graduate Fellowship for B. F. Carroll.

References

[1]Adamson, T. C., and Messiter, A. F., "Analysis of Two-Dimensional Interactions Between Shock Waves and Boundary Layers," *Annual Review of Fluid Mechanics*, Vol. 12, Annual Reviews, Palo Alto, CA, 1980, pp. 103–138.

[2]Green, J. E., "Interactions Between Shock Waves and Turbulent Boundary Layers," *Progress in Aerospace Sciences*, Vol. 11, Pergamon, Oxford, England, UK, 1970, pp. 235–341.

[3]Lustwerk, F., "The Influence of Boundary Layer on the 'Normal' Shock Configuration," Massachusetts Inst. of Technology Guided Missiles Program, Cambridge, MA, METEOR Rept. 61, Sept. 1950.

[4]Carroll, B. F., and Dutton, J. C., "Characteristics of Multiple Shock Wave/Turbulent Boundary Layer Interactions in Rectangular Ducts," *Journal of Propulsion and Power*, Vol. 6, No. 2, 1990, pp. 186–193.

[5]Ikui, T., Matsuo, K., and Nagai, M., "The Mechanisms of Psuedo-Shock Waves," *Bulletin of the Japan Society of Mechanical Engineers*, Vol. 17, No. 108, 1974, pp. 731–739.

[6]Ikui, T., Matsuo, K., Nagai, M., and Honjo, M., "Oscillation Phenomena of Psuedo-Shock Waves," *Bulletin of the Japan Society of Mechanical Engineers*, Vol. 17, No. 112, 1974, pp. 1278–1285.

[7]Om, D., and Childs, M. E., "An Experimental Investigation on Multiple Shock Wave/Turbulent Boundary Layer Interactions in a Circular Duct," *AIAA Journal*, Vol. 23, No. 10, 1985, pp. 1506–1511.

[8]Chriss, R. M., Keith, T. G., Jr., Hingst, W. R., Strazisar, A. J., and Porro, A. R., "An LDA Investigation of Three-Dimensional Normal Shock-Boundary Layer Interactions in a Corner," AIAA Paper 87-1369, June 1987.

[9]Sajben, M., Morris, M. J., Bogar, T. J., and Kroutil, J. C., "Confined Normal-Shock/Turbulent-Boundary-Layer Interaction Followed by an Adverse Pressure Gradient," AIAA Paper 89-0354, Jan. 1989.

[10]Delery, J. M., "Experimental Investigation of Turbulence Properties in Transonic Shock/Boundary Layer Interactions," *AIAA Journal*, Vol. 21, No. 2, 1983, pp. 180–185.

[11]East, L. F., "The Application of a Laser Anemometer to the Investigation of Shock-Wave Boundary Layer Interactions," (NATO) AGARD CP 193, May 1976.

[12]Mateer, G. G., Brosch, A., and Viegas, J. R., "A Normal Shock-Wave Turbulent Boundary Layer Interaction at Transonic Speeds," AIAA Paper 76-161, Jan. 1976.

[13]Carroll, B. F., and Dutton, J. C., "A Numerical and Experimental Investigation of Multiple Shock Wave/Turbulent Boundary Layer Interactions in a Rectangular Duct," Dept. of Mechanical and Industrial Engineering, Univ. of Illinois at Urbana-Champaign, Urbana, IL, Rept. UILU ENG 88-4015, Aug. 1988.

[14]Carroll, B. F., and Dutton, J. C., "An LDV Investigation of a Multiple Normal Shock Wave/Turbulent Boundary Layer Interaction," AIAA Paper 89-0355, Jan. 1989; also *Journal of Propulsion and Power* (to be published).

[15]Mateer, G. G., and Viegas, J. R, "Effect of Mach and Reynolds Numbers on a Normal Shock-Wave/Turbulent Boundary-Layer Interaction," AIAA Paper 79-1502, July 1979.

[16]Dolling, D. S., and Murphy, M. T., "Unsteadiness of the Separated Shock Wave Structure in a Supersonic Compression Ramp Flowfield," *AIAA Journal*, Vol. 21, No. 12, 1983, pp. 1628–1634.